JACS
JOURNAL OF THE AMERICAN CHEMICAL SOCIETY
pubs.acs.org/JACS
Article

# Total Synthesis and Target Identification of the Curcusone Diterpenes

Chengsen Cui,[$] Brendan G. Dwyer,[$] Chang Liu, Daniel Abegg, Zhong-Jian Cai, Dominic G. Hoch, Xianglin Yin, Nan Qiu, Jie-Qing Liu, Alexander Adibekian,[*] and Mingji Dai[*]

Cite This: *J. Am. Chem. Soc.* 2021, 143, 4379–4386
Read Online
ACCESS | Metrics & More | Article Recommendations | Supporting Information

**ABSTRACT:** The curcusone natural products are complex diterpenes featuring a characteristic [6−7−5] tricyclic carbon skeleton similar to the *daphnane* and *tigliane* diterpenes. Among them, curcusones A−D demonstrated potent anticancer activity against a broad spectrum of human cancer cell lines. Prior to this study, no total synthesis of the curcusones was achieved and their anticancer mode of action remained unknown. Herein, we report our synthetic and chemoproteomics studies of the curcusone diterpenes which culminate in the first total synthesis of several curcusone natural products and identification of BRCA1-associated ATM activator 1 (BRAT1) as a cellular target. Our efficient synthesis is highly convergent, builds upon cheap and abundant starting materials, features a thermal [3,3]-sigmatropic rearrangement and a novel $FeCl_3$-promoted cascade reaction to rapidly construct the critical cycloheptadienone core of the curcusones, and led us to complete the first total synthesis of curcusones A and B in only 9 steps, C and D in 10 steps, and dimericursone A in 12 steps. The chemical synthesis of dimericursone A from curcusones C and D provided direct evidence to support the proposed Diels−Alder dimerization and cheletropic elimination biosynthetic pathway. Using an alkyne-tagged probe molecule, BRAT1, an important but previously "undruggable" oncoprotein, was identified as a key cellular target via chemoproteomics. We further demonstrate for the first time that BRAT1 can be inhibited by curcusone D, resulting in impaired DNA damage response, reduced cancer cell migration, potentiated activity of the DNA damaging drug etoposide, and other phenotypes similar to BRAT1 knockdown.

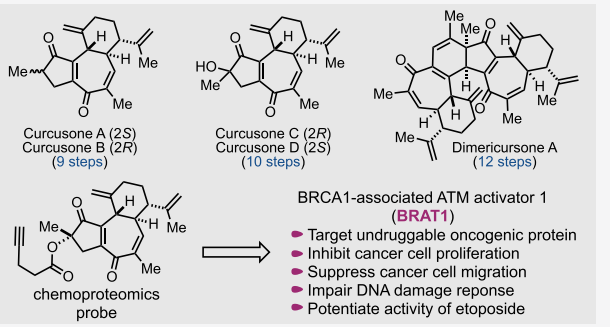


## INTRODUCTION

Natural products have been valuable sources and inspirations of lifesaving drug molecules.[1] Their accumulated evolutionary wisdom together with their structural novelty and diversity make them unparalleled for novel therapeutic development. However, their natural scarcity, structural complexity, and unknown mode of action often hamper their further development in the drug discovery pipeline. Total synthesis has been employed as one way to solve the material supply and chemical probe synthesis for comprehensive biological profiling and target identification.[2] Meanwhile, many biologically validated disease targets are considered as "undruggable" from a chemical standpoint due to the lack of enzymatic activity and/or small molecule binding sites.[3] The BRCA1-associated ATM activator 1 (BRAT1) protein has been validated as an oncogenic protein involved in various cancers but belongs to the "undruggable" category with no known small molecule inhibitors to date. Herein, we report a collaborative effort in the total synthesis and target identification of the curcusone natural products which yielded the first total synthesis of curcusones A and B in 9 steps, C and D in 10 steps, and dimericursone A in 12 steps and revealed BRAT1 as a key cellular target of the curcusones.

The curcusone diterpenes (Figure 1A) were isolated from *Jatropha curcas*, a widely used ingredient in traditional remedies for a variety of ailments including cancer. Structurally, they share a characteristic [6−7−5] tricyclic carbon skeleton with the *daphnane* and *tigliane* diterpenes.[4] Curcusones A−D (**1a**−**d**), isolated by Clardy and co-workers in 1986, were unambiguously identified as two epimeric pairs at the C2 position.[5] Since then, around 30 curcusone molecules have been isolated including curcusones F−J,[6] which lack the dienone moiety in the seven-membered ring. Structurally rearranged analogs like spirocurcasone (**3**) and dimeric analogs such as dimericursone A (**2a**) and dimericursone B (**2b**) were discovered recently.[7,8] Among

Received: January 16, 2021
Published: March 11, 2021

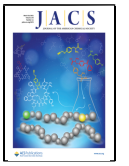







https://dx.doi.org/10.1021/jacs.1c00557
*J. Am. Chem. Soc.* 2021, 143, 4379−4386

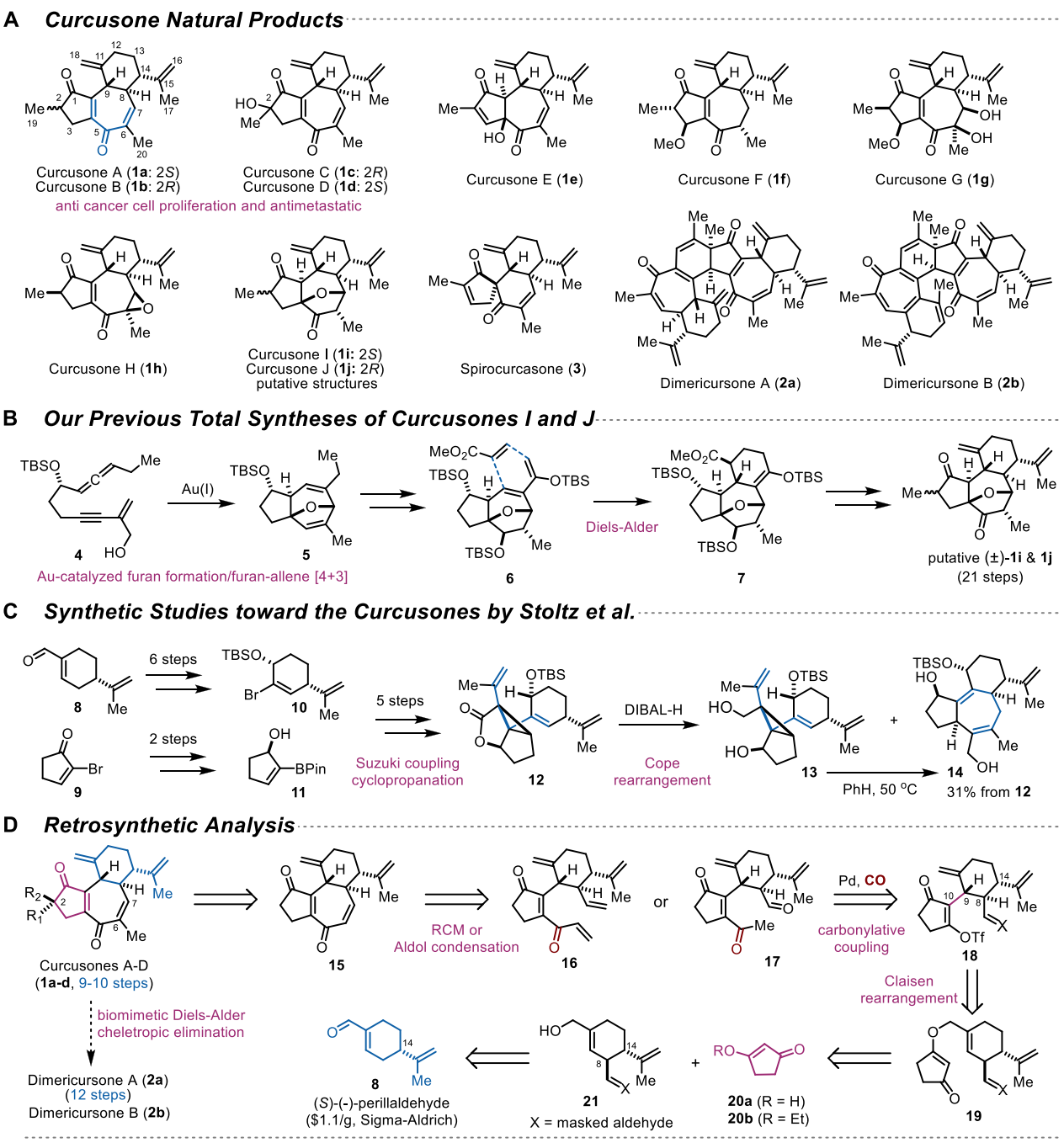


**Figure 1.** Curcusone diterpenes and their synthesis.

them, curcusones A–D (**1a–1d**) exhibited low micromolar $IC_{50}$ values against a broad spectrum of human cancer cell lines.[6] However, no total syntheses of curcusones A–D (**1a–1d**) and their dimeric products (**2a** and **2b**) were reported, prior to this study, and their mode of action remained unknown.

While the closely related *daphnane* and *tigliane* diterpenes have attracted a significant amount of synthetic interest,[9] the curcusone molecules have surprisingly received little attention despite their therapeutic potential. In 2017, we reported the first total syntheses of the putative structures of curcusones I and J (**1i** and **1j**) in 21 steps (Figure 1B), ultimately leading to the conclusion that the originally proposed structures of both **1i** and **1j** were incorrect.[10] Our synthesis involves a gold-catalyzed tandem furan formation and furan-allene [4 + 3] cycloaddition to build the 5,7-fused ring system with an oxa bridge and a Diels–Alder reaction to construct the 6-membered ring. In 2019, Stoltz and co-workers reported their studies toward synthesizing **1a–1d** (Figure 1C).[11] Their approach features an elegant divinylcyclopropane-cycloheptadiene rearrangement to forge the 7-membered ring and reaches advanced intermediate **14** after 12 steps from **8**.

Our ongoing interest in natural products that can covalently modify cellular proteins[12] prompted us to continue pursuing the total synthesis and target identification of curcusones A–D (**1a–1d**) with an electrophilic cycloheptadienone moiety. This unique structural feature could allow them to form a covalent bond with the nucleophilic residues of certain cellular


https://dx.doi.org/10.1021/jacs.1c00557
J. Am. Chem. Soc. 2021, 143, 4379–4386

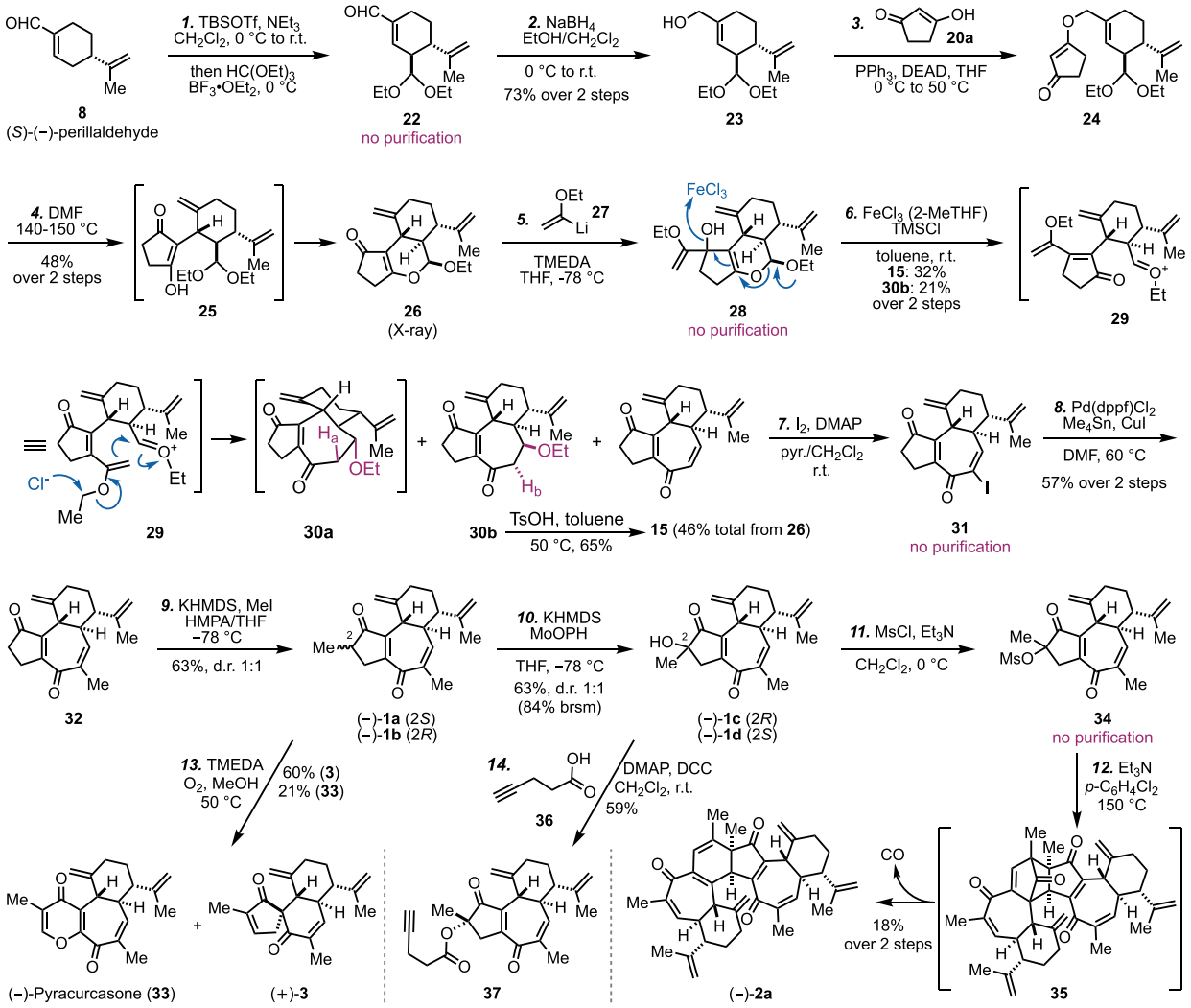


**Figure 2.** Total syntheses of curcusones A−D, dimericursone A, and their analogs.

proteins.[13] Previous cytotoxicity studies found that reduction and/or oxidation of the C6−C7 double bond greatly reduced their anticancer activity.[6] As such, an approach allowing variation of the C6 and C7 substituents would be highly desirable. We envisioned **15** as an advanced intermediate (Figure 1D). $\alpha$-Halogenation followed by two methylation reactions would lead to **1a** and **1b**, which could be oxidized to **1c** and **1d** via $\alpha$-hydroxylation. A ring closing metathesis (RCM) or an intramolecular aldol condensation was planned to form the 7-membered dienone (**16**/**17** → **15**). Both **16** and **17** could be prepared from vinyl triflate **18** via Pd-catalyzed carbonylative cross couplings. At this stage, disconnection of the C9−C10 bond could break **18** into two simple pieces, but a direct intermolecular C−C bond formation to construct such a bond is challenging. Thus, we opted for a Claisen rearrangement to forge this C−C bond in a stereoselective manner and designed **19** with a masked aldehyde as the Claisen rearrangement precursor. **19** could be assembled from simple building blocks **20a**/**20b** and **21**. The latter could be derived from a cheap chiral pool molecule (*S*)-(−)-perillaldehyde **8**.

## RESULTS

**Total Synthesis.** Our synthesis started with preparing **23** (Figure 2), a known compound synthesized from **8** in three steps−extended silyl enol ether formation, vinylogous Mukaiyama aldol reaction, and $NaBH_4$ reduction.[14] We combined the first two steps into a one-pot reaction; crude **22** was then subjected to $NaBH_4$ reduction directly to produce multidecagram scale of **23** in one batch. We next needed to prepare **24** for the Claisen rearrangement. NaH-promoted addition−elimination between **23** and **20b** afforded **24**, albeit in low yield (35%). We then used a Mitsunobu reaction between **23** and **20a** to prepare **24**, but the hydrazine byproduct derived from diethyl azodicarboxylate could not be separated from **24**. The recently reported redox-neutral organocatalytic Mitsunobu conditions were also explored but failed to provide **24**.[15] Fortunately, the hydrazine byproduct could be tolerated in the Claisen rearrangement. After **24** was heated at 140−150 °C in DMF for 18 h, the Claisen rearrangement did occur, but the rearranged product **25** further cyclized to provide tricyclic compound **26** (CCDC 2033828) as a single diastereomer in 48% yield from **23**.

To avoid further cyclization with the acetal group, we sought to use a more stable protecting group for the aldehyde and converted **23** to thioacetal **38** (Figure 3). With a more stable


https://dx.doi.org/10.1021/jacs.1c00557
J. Am. Chem. Soc. 2021, 143, 4379−4386

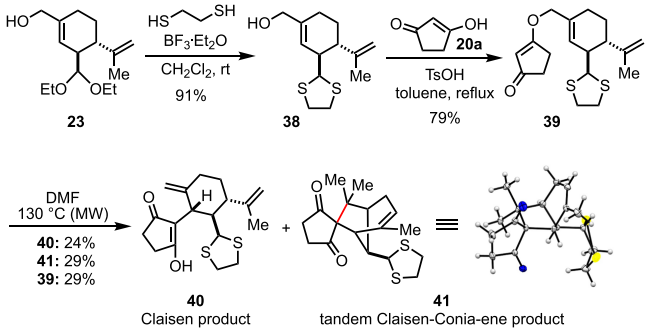


**Figure 3.** Investigation of the Claisen rearrangement.

thioacetal, TsOH-catalyzed addition−elimination could be used to prepare the new Claisen rearrangement precursor **39** in 79% yield. Interestingly, upon the microwave-heating of **39** in DMF at 130 °C, in addition to the desired rearrangement product **40** (24% yield), a 29% yield of byproduct **41** was obtained and an equal amount of **39** was recovered. The structure of **41** was unambiguously established by X-ray crystallography analysis (CCDC 2055698). Mechanistically, **41** was produced from **39** via a remarkable tandem Claisen rearrangement and thermal Conia ene reaction. We tried to suppress the formation of **41** by shortening the reaction time or lowering the reaction temperature, but these efforts led to overall decreased yield of **40**.

We then decided to continue with **26** and explore the hidden cyclopentane-1,3-dione symmetry to synthesize **17**. We started with investigating the 1,2-addition of lithiated ethyl vinyl ether (**27**) to **26** theorizing that a global hydrolysis would release the methyl ketone and the aldehyde at once to form **17** for the aldol condensation. This 1,2-addition turned out to be nontrivial. When two equiv. of **27** was used, only less than 10% yield of **28** was obtained. Owing to their oxophilicity, cerium chloride and lanthanum chloride have been used to promote 1,2-additions.[16] Unfortunately, both failed in our case. Eventually, the 1,2-addition was improved by increasing the amount of **27** to 10 equiv.,[17] and **28** was prepared in 57% yield. **28** was then subjected to hydrolysis upon the treatment with TsOH, and **17** was obtained in 51% yield from **26**. Meanwhile, we were delighted to observe the formation of **15** in the same reaction, albeit in very poor yield (<5%). We were encouraged to achieve a global hydrolysis/aldol condensation cascade to synthesize **15** from **28** in one step and identified $FeCl_3$[18] in combination with TMSCl as the optimal conditions. When crude **28** was treated with a premixed $FeCl_3$ (0.2 M in 2-methyltetrahydrofuran) and TMSCl in toluene at room temperature, desired product **15** was produced in 32% yield from **26** together with 21% of **30b**. The failure of converting **17** to **15** with $FeCl_3$ and the isolation of **30b** led us to propose that the $FeCl_3$/TMSCl-promoted cascade process went through intermediates **29** and **30a** to form **15** in one step. In intermediate **30a**, the $\alpha$-$H_a$ and the EtO group are antiperiplanar, thus the subsequent 1,2-elimination is facile and occurred under the $FeCl_3$/TMSCl conditions. In intermediate **30b**, $\alpha$-$H_b$ and the EtO group are both in the pseudo equatorial positions, which was supported by NMR analysis and computational modeling. Therefore, its conversion to **15** is more difficult. In order to maximize the overall yield of

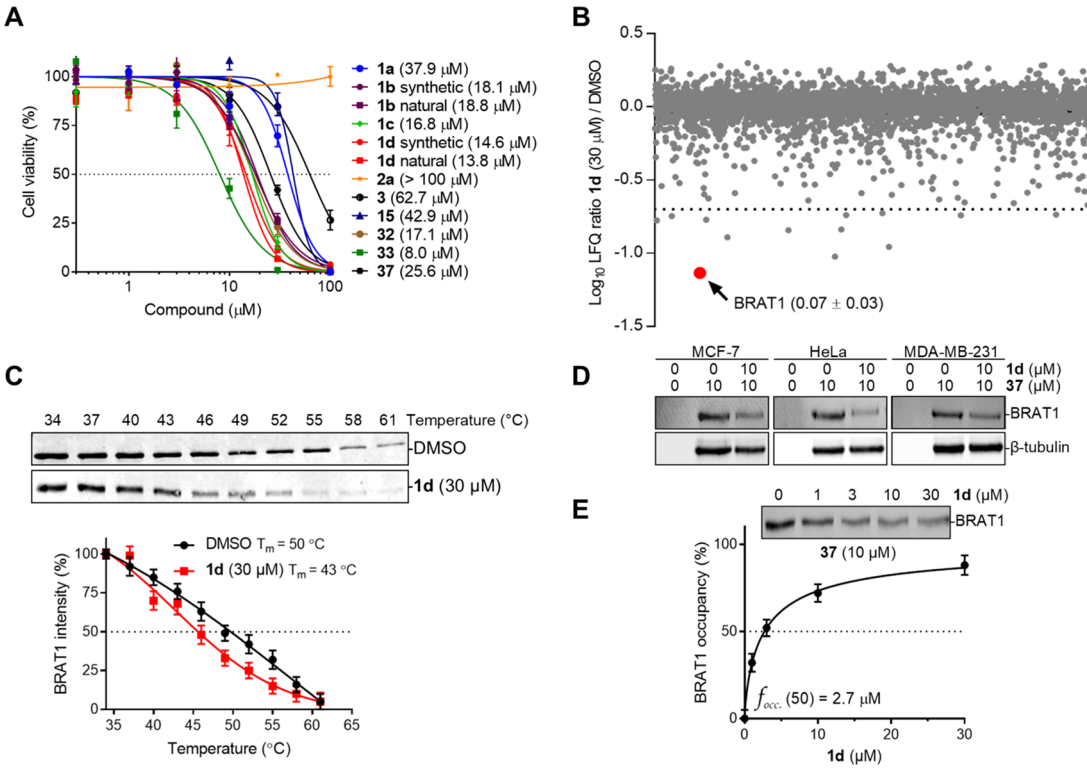


**Figure 4.** Identification of BRAT1 as a cellular target of **1d**. (A) Viability of MCF-7 cells following 24 h compound treatment with $EC_{50}$ values in brackets ($n$ = 3). (B) Scatter plot of proteins competed by **1d** from probe **37** (10 $\mu$M) enrichment in MCF-7 cells with BRAT1 highlighted ($n$ = 3). (C) Western blot (top) and quantification (bottom) of thermal shift assay of overexpressed FLAG-BRAT1 lysate treated with **1d**. (D) Western blots of BRAT1 following treatment of live cells with **1d** and enrichment by **37** in competitive pulldown assays. (E) Western blot (top) and quantification (bottom) of BRAT1 pulldown with **37** in HeLa cells and dose-dependent competition with **1d**. All error bars are SD.



https://dx.doi.org/10.1021/jacs.1c00557
J. Am. Chem. Soc. 2021, 143, 4379−4386

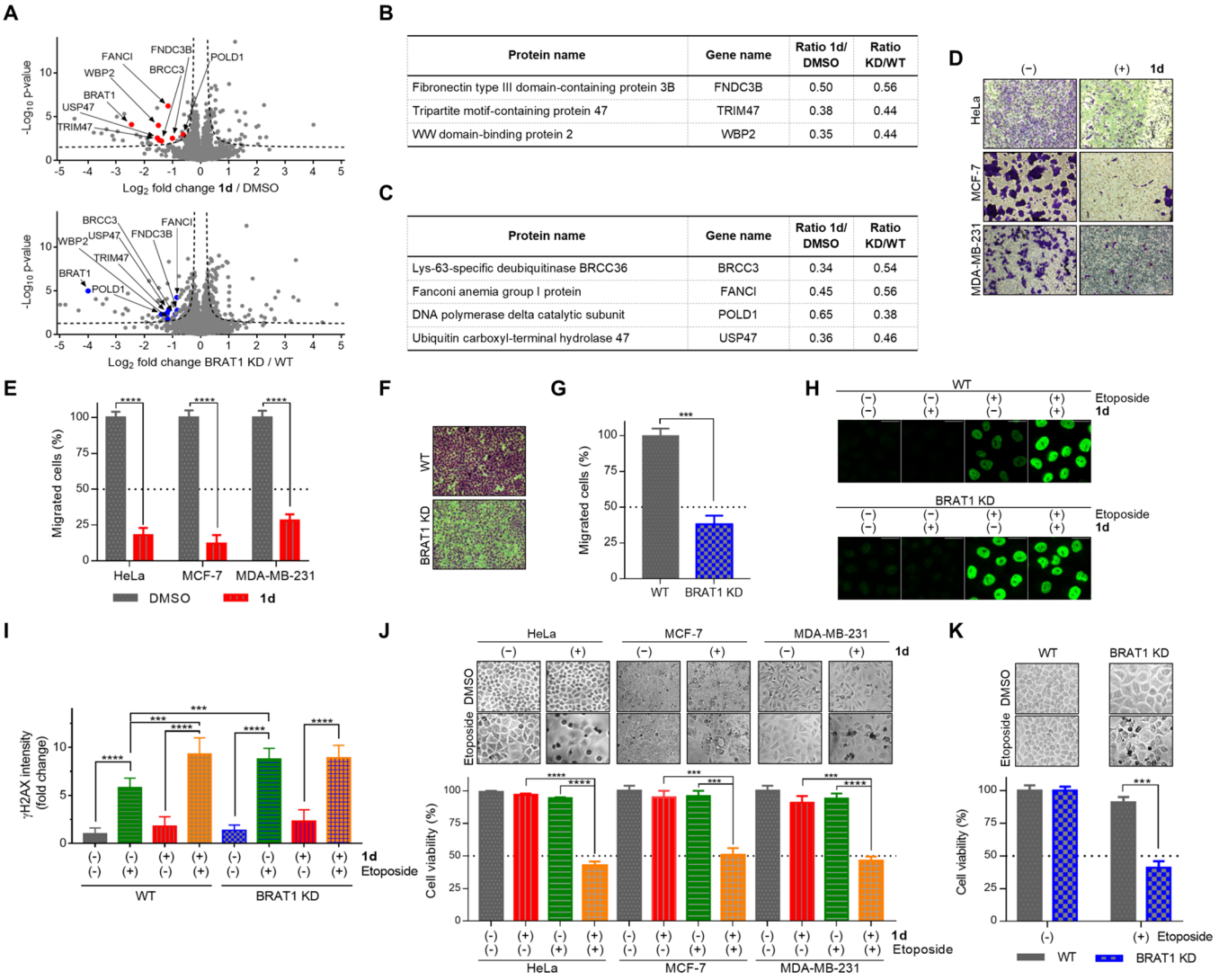


| Protein name | Gene name | Ratio 1d/ DMSO | Ratio KD/WT |
|---|---|---|---|
| Fibronectin type III domain-containing protein 3B | FNDC3B | 0.50 | 0.56 |
| Tripartite motif-containing protein 47 | TRIM47 | 0.38 | 0.44 |
| WW domain-binding protein 2 | WBP2 | 0.35 | 0.44 |

| Protein name | Gene name | Ratio 1d/ DMSO | Ratio KD/WT |
|---|---|---|---|
| Lys-63-specific deubiquitinase BRCC36 | BRCC3 | 0.34 | 0.54 |
| Fanconi anemia group I protein | FANCI | 0.45 | 0.56 |
| DNA polymerase delta catalytic subunit | POLD1 | 0.65 | 0.38 |
| Ubiquitin carboxyl-terminal hydrolase 47 | USP47 | 0.36 | 0.46 |

**Figure 5.** Evaluation of BRAT1 inactivation by **1d**. (A) Global proteomic analysis of HeLa cells comparing **1d** treatment to BRAT1 knockdown versus DMSO or nontargeting (WT) controls, respectively. Color dots indicate proteins which are downregulated in both conditions ($n$ = 3). (B) Table showing common downregulated proteins involved in cell migration and, (C) in DNA repair. (D) Crystal violet images and, (E) quantification of cells in a transwell migration assay following **1d** (1 $\mu$M; 24 h) treatment ($n$ = 3). (F) Crystal violet images and, (G) quantification of WT and BRAT1 KD cells (24 h) in a transwell migration assay ($n$ = 3). (H) Fluorescence microscopy images and, (I) quantification of WT or BRAT1 KD cells treated with DMSO, **1d** (3 $\mu$M), etoposide (30 $\mu$M), or both compounds showing $\gamma$H2AX staining ($n$ = 3). (J) Images of cells (top) and quantification (bottom) after 24 h treatment with DMSO, **1d** (3 $\mu$M), etoposide (50 $\mu$M), or both compounds or, (K) following BRAT1 knockdown and subsequent treatment with etoposide. All error bars are SD. All scale bars indicate 30 $\mu$m. ***$P$ < 0.001, ****$P$ < 0.0001, Welch's two-sided $t$ test.

**15**, we investigated conditions to promote the 1,2-elimination of **30b** and identified that it could be converted to **15** in 65% yield by heating with TsOH in toluene at 50 °C, which brings the overall yield of **15** from **26** to 46%.

With the [6−7−5] tricyclic carbon skeleton quickly assembled in only six steps, we next needed to introduce the two methyl groups. Johnson $\alpha$-iodination converted **15** to iodoenone **31**, which was surprisingly unstable. Therefore, after a quick workup, crude **31** was immediately subjected to the next Stille cross coupling with tetramethylstannane to provide **32** in 57% yield over two steps. Finally, $\alpha$-methylation of enone **32** at C2 position delivered a 1:1 mixture of separable (−)-curcusone A (**1a**) and (−)-curcusone B (**1b**) in 63% yield (9 steps total). $\alpha$-Hydroxylation of **1a** with KHDMS and MoOPH gave separable (−)-curcusone C (**1c**) and (−)-curcusone D (**1d**) in 63% yield (d.r. 1:1; 84% brsm; 10 steps total). Additionally, in order to obtain analogs for biological activity comparison, we converted (−)-**1b** to (+)-spirocurcasone (**3**) and (−)-**33** (a synthetic derivative named as pyracurcasone) by following a reported one-step procedure.[7] The $^{1}$H, $^{13}$C NMR, and other analytic data of our synthetic samples matched well with the reported ones, which also conclude that the absolute configuration of **1a**−**1d** assigned by Clardy et al. in 1986 is opposite of the actual ones.

We then set out to synthesize dimericursone A (**2a**) from **1a**−**1d** via a biomimetic dimerization. The proposed biosynthesis of **2a** consists of a sequence of oxidative dehydrogenation of **1a**/**1b** or dehydration of **1c**/**1d** to form a reactive cyclopentadienone intermediate followed by Diels−Alder dimerization and cheletropic extrusion of carbon monoxide.[8] From there, **2a** could be converted to **2b** via another oxidative dehydrogenation and double bond isomerization. We started


https://dx.doi.org/10.1021/jacs.1c00557
J. Am. Chem. Soc. 2021, 143, 4379−4386

with **1c** and **1d**. After an unfruitful attempt to synthesize **2a** using direct heat at elevated temperatures, we first converted their 1:1 mixture to their mesylates (**34**). After extensive exploration, we realized that the use of triethylamine as a base in 1,4-dichlorobenzene at 150 °C led to the production of (−)-**2a** in 18% yield over two steps, which provides direct evidence in support of the proposed biosynthetic pathway. Under our conditions, the formation of **2b** was not observed.

**Probe Synthesis.** To elucidate the anticancer mechanism and identify potential cellular targets of curcusones, an alkyne-tagged probe molecule **37** was designed for chemoproteomics studies. Since the dienone is likely protein-reactive and is critical for the observed activity, we decided to minimize the structural perturbation of this part and used the tertiary alcohol as a handle to link with a terminal alkyne. **37** was synthesized in 59% yield from (−)-**1d** via a DCC-promoted coupling with **36**.

**Cytotoxicity and Target Identification.** We evaluated the cytotoxicity of curcusones and their analogs in breast cancer MCF-7 cells using the WST-1 assay (Figure 4A; see Table S1 for structures and $EC_{50}$ values). Synthetic **1a**−**1d**, natural **1b** and **1d**, and intermediates **15** and **32** exhibited micromolar $EC_{50}$ values against MCF-7 cells with **1d** being the most potent curcusone. Importantly, the cytotoxicity values for synthetic **1b** and **1d** were virtually identical to the values of their naturally isolated counterparts. Analog **33** showed slightly better antiproliferation activity indicating the feasibility of finely tuning the cycloheptadienone moiety to improve potency, but **2a** was not active even at 100 $\mu$M. Likely due to the full confluency of the tested MCF-7 cells, the $EC_{50}$ values we obtained were about 1 order of magnitude higher than previously reported (1.6−3.1 $\mu$M $EC_{50}$ values for **1a**−**1d**).[6] Gratifyingly, **37** retained similar anticancer properties of **1d**, thus warranting its use in competitive chemoproteomic studies.

We then identified the cellular targets of curcusones by competitive chemoproteomics using probe **37**. MCF-7 cells were treated with **1d** or DMSO for 4 h followed by lysis, treatment with **37**, CuAAC with biotin azide, enrichment, digestion, and LC-MS/MS analysis using label-free quantification (Figure 4B and Table S2). The best competed target was BRAT1, which acts as a master regulator of the DNA damage response (DDR) and DNA repair by binding to BRCA1 and by activating DDR kinases such as ATM and PRKDC (DNA-PKcs) following DNA damage.[19−21] Knockdown of BRAT1 increased the constitutive level of apoptosis in human osteosarcoma cells[19] and decreased cancer cell proliferation and tumorigenicity *in vitro* and in mouse tumor xenografts.[21] BRAT1 is also an unfavorable prognostic marker in kidney and liver cancers.[22] Therefore, targeting BRAT1 is a promising strategy for cancer treatment.

We next characterized the physical interaction between **1d** and BRAT1. We overexpressed FLAG-BRAT1 in HEK-293T cells and performed a thermal shift assay by treating lysates with **1d**, heating as indicated, and probing the remaining soluble FLAG-BRAT1 by Western blotting (Figure 4C). We observed thermal destabilization of **1d**-treated BRAT1 indicating a direct interaction. To validate endogenous BRAT1 as a target of **1d** in live cells, we employed a competitive pulldown experiment. MCF-7 cells were treated with **1d** or DMSO for 4 h before lysis, treatment with probe **37**, CuAAC with biotin azide, streptavidin enrichment, elution, and Western blot visualization. Indeed, native BRAT1 was enriched by **37** and was competed by **1d** (Figure 4D). Additionally, **1d** competed the enrichment of BRAT1 from cervical cancer HeLa and triple negative breast cancer MDA-MB-231 cells, thus validating native BRAT1 as a cellular target of **1d** across these cell lines. To evaluate the binding reversibility, we performed a competitive BRAT1 pulldown assay with the irreversible cysteine-reactive probe iodoacetamide (IAA). HeLa lysate was treated with **37** (10 $\mu$M) for 1 h with either pre- or posttreatment with IAA (30 mM) for 1 h followed by enrichment and Western blot analysis as described above (Figure S1A). Indeed, both pre- and posttreatment with IAA competed BRAT1 enrichment by **37**, indicating that the curcusone probe forms a covalent bond with a cysteine in BRAT1 and this bond is reversible. We then treated live HeLa cells with different concentrations of **1d** for 4 h to evaluate BRAT1 target occupancy via our competitive pulldown assay, which revealed that **1d** reaches 50% fractional occupancy ($f_{occ.}(50)$) at 2.7 $\mu$M (Figure 4E). Collectively, these results demonstrate that **1d** is the first small-molecule binder of BRAT1.

**BRAT1 Modulation.** To determine whether **1d** inhibits BRAT1 in cells, we generated stable BRAT1 KD HeLa cells via shRNA retroviral transduction (Figure S1B). We then compared the protein expression profiles of BRAT1 KD cells versus **1d**-treated cells (3 $\mu$M, 24 h) by global proteomics analysis (Figure 5A−C and Table S3). Among 3347 quantified proteins in compound-treated cells, we found only 36 up- and 42 down-regulated proteins. Importantly, 31 of the 78 dysregulated proteins were also dysregulated in BRAT1 KD cells, thus indicating that **1d** functionally inhibits BRAT1 in cells. Notably, several well-known cancer migration and progression drivers were downregulated (Figure 5B), including TRIM47 which mediates cancer migration,[23] the bona fide oncoprotein and potential biomarker WBP2,[24] and the frequently highly amplified oncogene FNDC3B.[25] None of these proteins have previously been functionally linked to BRAT1. We then investigated the effect of **1d** treatment and BRAT1 KD on cancer cell migration in WT and BRAT1 KD HeLa cells, as well as WT MCF-7 and MDA-MB-231 cells (Figure 5D−G). As expected, BRAT1 knockdown greatly diminished migration of HeLa cells, and treatment with **1d** at 1 $\mu$M concentration also reduced migration of all cell lines by ∼4-fold.

Our global proteomics experiment also revealed several commonly downregulated key DNA repair proteins (Figure 5C) such as (i) POLD1 which synthesizes DNA during repair,[26] (ii) USP47 which facilitates base-excision repair,[27] (iii) FANCI which mediates the repair of DNA double strand breaks and interstrand cross-links,[28] and (iv) BRCC3 which stabilizes the accumulation of BRCA1 at DNA breaks.[29] These proteins have not been previously linked to BRAT1 either. Most notably, **1d** treatment (24 h) significantly downregulated the actual physical target, BRAT1 (ratio 0.18), as confirmed by Western blotting (Figure S1C). To evaluate whether this effect is due to proteasomal degradation or altered gene expression, we added the proteasome inhibitor MG132 for the final 4 h of **1d** treatment, which recovered BRAT1 protein levels. In contrast, when we measured *BRAT1* mRNA levels by RT-qPCR following **1d** treatment for 24 h (Figure S1D), we found no difference. Collectively, these findings demonstrate the importance of BRAT1 as a master regulator of the DDR and that **1d** inhibition of BRAT1 in cells induces proteasomal degradation over time.



https://dx.doi.org/10.1021/jacs.1c00557
J. Am. Chem. Soc. 2021, 143, 4379−4386

We then investigated whether **1d** would potentiate the DNA damaging effect of the clinical drug and topoisomerase inhibitor etoposide via BRAT1 inhibition. WT or BRAT1 KD HeLa cells were treated with DMSO, etoposide, **1d**, or etoposide and **1d** combined. Subsequent DNA damage was then measured by fluorescence microscopy using γH2AX staining (Figure 5H,I and Figure S1E). Treatment with **1d** (3 μM) or KD of BRAT1 alone did not increase γH2AX signal. However, cotreatment of **1d** with etoposide led to a 2-fold increase. Similarly, etoposide treatment significantly increased γH2AX signal in BRAT1 KD cells, recapitulating the **1d**/etoposide cotreatment results. Importantly, **1d** treatment did not increase γH2AX signal in etoposide-treated BRAT1 KD cells, confirming that the **1d**-etoposide synergism is linked to BRAT1 inactivation. Furthermore, cotreatment of **1d** with etoposide also increased cytotoxicity in HeLa, MCF-7, and MDA-MB-231 cells (Figure 5J). Likewise, there was increased cell death in BRAT1 KD HeLa cells following etoposide treatment relative to WT cells (Figure 5K). Altogether, these results demonstrate that targeting BRAT1 with **1d** is a promising anticancer strategy for chemosensitization to DNA damaging drugs.

In summary, we completed the first asymmetric total synthesis and target identification of the curcusone natural products. Our convergent synthesis builds upon a cheap and abundant chiral pool molecule (**8**) and features a thermal [3,3]-sigmatropic rearrangement and an $FeCl_3$-promoted global hydrolysis/aldol condensation cascade to rapidly construct the critical cycloheptadienone core. This efficient synthetic route yielded curcusones A and B (**1a** and **1b**) in only 9 steps, curcusones C and D (**1c** and **1d**) in 10 steps, and dimericursone A (**2a**) in 12 steps from (*S*)-(−)-**8**. The successful synthesis of **2a** from **1c**/**1d** experimentally supports the proposed Diels−Alder dimerization and cheletropic extrusion biosynthesis. By performing chemoproteomics with the alkyne probe **37**, we identified the previously "undruggable" oncogenic protein BRAT1 as a key cellular target of **1d**. Furthermore, **1d** inhibits BRAT1 in cancer cells, thereby reducing cancer cell migration, increasing susceptibility to DNA damage, and inducing chemosensitization to the approved drug etoposide. To our knowledge, **1d** is the first known small-molecule inhibitor of BRAT1, a master regulator of the DDR and DNA repair. Many promising clinical trials are underway targeting DDR proteins such as PARP, ATR, ATM, CHK, and DNA-PK as monotherapies or in combination with other treatments.[30] Olaparib, a PARP inhibitor, was approved by FDA in 2014 as a monotherapy to treat germline *BRCA1/2* mutant ovarian cancer.[30a] Our concise and convergent total synthesis has opened the gate for curcusone analog synthesis and structure−activity optimizations, which may thus yield novel BRTAT1 inhibitors as potential lead medicines for monotherapies or combination therapies.

## ■ ASSOCIATED CONTENT

### Supporting Information

The Supporting Information is available free of charge at https://pubs.acs.org/doi/10.1021/jacs.1c00557.

Experimental procedures and spectra data (PDF)
MS-based proteomic tables (XLSX)

### Accession Codes

CCDC 2033828 and 2055698 contain the supplementary crystallographic data for this paper. These data can be obtained free of charge via www.ccdc.cam.ac.uk/data_request/cif, or by emailing data_request@ccdc.cam.ac.uk, or by contacting The Cambridge Crystallographic Data Centre, 12 Union Road, Cambridge CB2 1EZ, UK; fax: +44 1223 336033.

## ■ AUTHOR INFORMATION


### Corresponding Authors

**Mingji Dai** − *Department of Chemistry and Center for Cancer Research, Purdue University, West Lafayette, Indiana 47907, United States;* orcid.org/0000-0001-7956-6426; Email: mjdai@purdue.edu

**Alexander Adibekian** − *Department of Chemistry, The Scripps Research Institute, Florida 33458, United States;* orcid.org/0000-0001-6453-0244; Email: aadibeki@scripps.edu

### Authors

**Chengsen Cui** − *Department of Chemistry and Center for Cancer Research, Purdue University, West Lafayette, Indiana 47907, United States;* orcid.org/0000-0002-6867-1826

**Brendan G. Dwyer** − *Department of Chemistry, The Scripps Research Institute, Florida 33458, United States*

**Chang Liu** − *Department of Chemistry and Center for Cancer Research, Purdue University, West Lafayette, Indiana 47907, United States*

**Daniel Abegg** − *Department of Chemistry, The Scripps Research Institute, Florida 33458, United States*

**Zhong-Jian Cai** − *Department of Chemistry and Center for Cancer Research, Purdue University, West Lafayette, Indiana 47907, United States*

**Dominic G. Hoch** − *Department of Chemistry, The Scripps Research Institute, Florida 33458, United States*

**Xianglin Yin** − *Department of Chemistry and Center for Cancer Research, Purdue University, West Lafayette, Indiana 47907, United States*

**Nan Qiu** − *Department of Chemistry, The Scripps Research Institute, Florida 33458, United States*

**Jie-Qing Liu** − *School of Medicine, Huaqiao University, Quanzhou 362021, P. R. China*

Complete contact information is available at: https://pubs.acs.org/10.1021/jacs.1c00557

### Author Contributions

[$]C.C. and B.G.D. contributed equally.


### Notes

The authors declare the following competing financial interest(s): M.D., A.A., C.C., B.G.D., Z.C. are inventors on patent application U.S. 63/084,594 submitted by Purdue University that covers the synthesis of curcusone derivatives.

## ■ ACKNOWLEDGMENTS

We thank Dr. Dany Pechalrieu for helpful discussions. We thank the NIH (R35 GM128570), the NSF Graduate Research Fellowships Program, the Reba and Nat Newman Endowed Fellowship, and The Scripps Research Institute for financial support. The NIH P30 CA023168 is acknowledged for supporting shared NMR resources to Purdue Center for Cancer Research. The XRD data is collected on a new single crystal X-ray diffractometer supported by the NSF through the Major Research Instrumentation Program under Grant No. CHE 1625543. This paper is dedicated to Professor Samuel J. Danishefsky on the occasion of his 85th birthday.



https://dx.doi.org/10.1021/jacs.1c00557
J. Am. Chem. Soc. 2021, 143, 4379−4386

## REFERENCES


(1) Harvey, A. L.; Edrada-Ebel, R.; Quinn, R. J. The re-emergence of natural products for drug discovery in the genomics era. *Nat. Rev. Drug Discovery* **2015**, *14*, 111−129.

(2) Nicolaou, K. C. Advancing the drug discovery and development process. *Angew. Chem., Int. Ed.* **2014**, *53*, 9128−9140.

(3) Dang, C. V.; Reddy, E. P.; Shokat, K. M.; Soucek, L. Drugging the 'undruggable' cancer targets. *Nat. Rev. Cancer* **2017**, *17*, 502−508.

(4) Wang, H. B.; Wang, X. Y.; Liu, L. P.; Qin, G. W.; Kang, T. G. Tigliane diterpenoids from the Euphorbiaceae and Thymelaeaceae families. *Chem. Rev.* **2015**, *115*, 2975−3011.

(5) Naengchomnong, W.; Thebtaranonth, Y.; Wiriyachitra, P.; Okamoto, K. T.; Clardy, J. Isolation and structure determination of four novel diterpenes from jatropha curcus. *Tetrahedron Lett.* **1986**, *27*, 2439−2442.

(6) Liu, J.-Q.; Yang, Y.-F.; Li, X.-Y.; Liu, E.-Q.; Li, Z.-R.; Zhou, L.; Li, Y.; Qiu, M.-H. Cytotoxicity of naturally occurring rhamnofolane diterpenes from Jatropha curcas. *Phytochemistry* **2013**, *96*, 265−272.

(7) Li, X.-Y.; Yang, Y.-F.; Peng, X.-R.; Li, M.-M.; Li, L.-Q.; Deng, X.; Qin, H.-B.; Liu, J.-Q.; Qiu, M.-H. One-step semisynthesis method of spirocurcasone and pyracurcasone from curcusones A and B. *Org. Lett.* **2014**, *16*, 2196−2199.

(8) Liu, J.-Q.; Xu, Y.; Xiao, Q.; Huang, J.-D.; Ma, J.-J.; Lian, C.-L.; Huang, M.-Y.; Du, Z.; Wang, C.-F. Dimericursones A and B: two unprecedented hexacyclic dimeric diterpenoids from the root barks of Jatropha curcas. *Org. Biomol. Chem.* **2018**, *16*, 8305−8310.

(9) For selected examples: (a) Wender, P. A.; Jesudason, C. D.; Nakahira, H.; Tamura, N.; Tebbe, A. L.; Ueno, Y. The first synthesis of a daphnane diterpene: The enantiocontrolled total synthesis of (+)-resiniferatoxin. *J. Am. Chem. Soc.* **1997**, *119*, 12976−12977. (b) Hashimoto, S.; Katoh, S. I.; Kato, T.; Urabe, D.; Inoue, M. Total Synthesis of Resiniferatoxin Enabled by Radical-Mediated Three-Component Coupling and 7-endo Cyclization. *J. Am. Chem. Soc.* **2017**, *139*, 16420−16429. (c) Wender, P. A.; Rice, K. D.; Schnute, M. E. The first formal asymmetric synthesis of phorbol. *J. Am. Chem. Soc.* **1997**, *119*, 7897−7898. (d) Kawamura, S.; Chu, H.; Felding, J.; Baran, P. S. Nineteen-step total synthesis of (+)-phorbol. *Nature* **2016**, *532*, 90−93. (e) Wender, P. A.; Kee, J. M.; Warrington, J. M. Practical synthesis of prostratin, DPP, and their analogs, adjuvant leads against latent HIV. *Science* **2008**, *320*, 649−652. (f) Lee, K.; Cha, J. K. Formal synthesis of (+)-phorbol. *J. Am. Chem. Soc.* **2001**, *123*, 5590−5591. (g) Asaba, T.; Katoh, Y.; Urabe, D.; Inoue, M. Total Synthesis of Crotophorbolone. *Angew. Chem., Int. Ed.* **2015**, *54*, 14457−14461. (h) Tong, G. H.; Liu, Z.; Li, P. F. Total Synthesis of (±)-Prostratin. *Chem.* **2018**, *4*, 2944−2954. (i) Yu, T.; Sun, Y.; Tu, C.; Chen, T.; Fu, S.; Liu, B. Total synthesis of crotophorbolone. *Chem. Sci.* **2020**, *11*, 7177−7181.

(10) Li, Y.; Dai, M. Total Syntheses of the Reported Structures of Curcusones I and J through Tandem Gold Catalysis. *Angew. Chem., Int. Ed.* **2017**, *56*, 11624−11627.

(11) (a) Lee, C. W.; Taylor, B. L. H.; Petrova, G. P.; Patel, A.; Morokuma, K.; Houk, K. N.; Stoltz, B. M. An Unexpected Ireland-Claisen Rearrangement Cascade During the Synthesis of the Tricyclic Core of Curcusone C: Mechanistic Elucidation by Trial-and-Error and Automatic Artificial Force-Induced Reaction (AFIR) Computations. *J. Am. Chem. Soc.* **2019**, *141*, 6995−7004. (b) Wright, A. C.; Lee, C. W.; Stoltz, B. M. Progress toward the Enantioselective Synthesis of Curcusones A-D via a Divinylcyclopropane Rearrangement Strategy. *Org. Lett.* **2019**, *21*, 9658−9662. (c) Wright, A. C.; Stoltz, B. M. Enantioselective construction of the tricyclic core of curcusones A-D via a cross-electrophile coupling approach. *Chem. Sci.* **2019**, *10*, 10562−10565.

(12) Davis, D. C.; Hoch, D. G.; Wu, L.; Abegg, D.; Martin, B. S.; Zhang, Z.-Y.; Adibekian, A.; Dai, M. Total Synthesis, Biological Evaluation, and Target Identification of Rare Abies Sesquiterpenoids. *J. Am. Chem. Soc.* **2018**, *140*, 17465−17473.

(13) Jackson, P. A.; Widen, J. C.; Harki, D. A.; Brummond, K. M. Covalent Modifiers: A Chemical Perspective on the Reactivity of $\alpha,\beta$-Unsaturated Carbonyls with Thiols via Hetero-Michael Addition Reactions. *J. Med. Chem.* **2017**, *60*, 839−885.

(14) Abe, H.; Sato, A.; Kobayashi, T.; Ito, H. Concise total synthesis of spirocurcasone. *Org. Lett.* **2013**, *15*, 1298−1301.

(15) Beddoe, R. H.; Andrews, K. G.; Magne, V.; Cuthbertson, J. D.; Saska, J.; Shannon-Little, A. L.; Shanahan, S. E.; Sneddon, H. F.; Denton, R. M. Redox-neutral organocatalytic Mitsunobu reactions. *Science* **2019**, *365*, 910−914.

(16) Krasovskiy, A.; Kopp, F.; Knochel, P. Soluble lanthanide salts ($LnCl_3 \cdot 2$ LiCl) for the improved addition of organomagnesium reagents to carbonyl compounds. *Angew. Chem., Int. Ed.* **2006**, *45*, 497−500.

(17) Haelsig, K. T.; Xuan, J.; Maimone, T. J. Total Synthesis of (−)-Curvulamine. *J. Am. Chem. Soc.* **2020**, *142*, 1206−1210.

(18) Ludwig, J. R.; Zimmerman, P. M.; Gianino, J. B.; Schindler, C. S. Iron(III)-catalyzed carbonyl-olefin metathesis. *Nature* **2016**, *533*, 374−370.

(19) Aglipay, J. A.; Martin, S. A.; Tawara, H.; Lee, S. W.; Ouchi, T. ATM activation by ionizing radiation requires BRCA1-associated BAAT1. *J. Biol. Chem.* **2006**, *281*, 9710−9718.

(20) So, E. Y.; Ouchi, T. Functional interaction of BRCA1/ATM-associated BAAT1 with the DNA-PK catalytic subunit. *Exp. Ther. Med.* **2011**, *2*, 443−447.

(21) So, E. Y.; Ouchi, T. BRAT1 deficiency causes increased glucose metabolism and mitochondrial malfunction. *BMC Cancer* **2014**, *14*, 548.

(22) The Human Protein Atlas. < https://www.proteinatlas.org/ENSG00000106009-BRAT1/pathology> (accessed 2020−08−13), BRAT1: Pathology.

(23) Han, Y.; Tian, H.; Chen, P.; Lin, Q. TRIM47 overexpression is a poor prognostic factor and contributes to carcinogenesis in non-small cell lung carcinoma. *Oncotarget* **2017**, *8*, 22730−22740.

(24) Tabatabaeian, H.; Rao, A.; Ramos, A.; Chu, T.; Sudol, M.; Lim, Y. P. *Oncogene* **2020**, *39*, 4621−4635.

(25) Chen, C.-F.; Hsu, E.-C.; Lin, K.-T.; Tu, P.-H.; Chang, H.-W.; Lin, C.-H.; Chen, Y.-J.; Gu, D.-L.; Lin, C.-H.; Wu, J.-Y.; Chen, Y.-T.; Hsu, M.-T.; Jou, Y.-S. Overlapping high-resolution copy number alterations in cancer genomes identified putative cancer genes in hepatocellular carcinoma. *Hepatology* **2010**, *52*, 1690−1701.

(26) Nicolas, E.; Golemis, E. A.; Arora, S. POLD1: Central mediator of DNA replication and repair, and implication in cancer and other pathologies. *Gene* **2016**, *590*, 128−141.

(27) Nickson, C. M.; Parsons, J. L. Monitoring regulation of DNA repair activities of cultured cells in-gel using the comet assay. *Front. Genet.* **2014**, *5*, 232.

(28) Smogorzewska, A.; Matsuoka, S.; Vinciguerra, P.; McDonald, E. R., 3rd; Hurov, K. E.; Luo, J.; Ballif, B. A.; Gygi, S. P.; Hofmann, K.; D'Andrea, A. D.; Elledge, S. J. Identification of the FANCI protein, a monoubiquitinated FANCD2 paralog required for DNA repair. *Cell* **2007**, *129*, 289−301.

(29) Dong, Y.; Hakimi, M.-A.; Chen, X.; Kumaraswamy, E.; Cooch, N. S.; Godwin, A. K.; Shiekhattar, R. Regulation of BRCC, a holoenzyme complex containing BRCA1 and BRCA2, by a signalosome-like subunit and its role in DNA repair. *Mol. Cell* **2003**, *12*, 1087−1099.

(30) (a) Pearl, L. H.; Schierz, A. C.; Ward, S. E.; Al-Lazikani, B.; Pearl, F. M. Therapeutic opportunities within the DNA damage response. *Nat. Rev. Cancer* **2015**, *15*, 166−180. (b) de Bono, J.; Mateo, J.; Fizazi, K.; Saad, F.; Shore, N.; Sandhu, S.; Chi, K. N.; Sartor, O.; Agarwal, N.; Olmos, D.; Thiery-Vuillemin, A.; Twardowski, P.; Mehra, N.; Goessl, C.; Kang, J.; Burgents, J.; Wu, W.; Kohlmann, A.; Adelman, C. A.; Hussain, M. Olaparib for Metastatic Castration-Resistant Prostate Cancer. *N. Engl. J. Med.* **2020**, *382*, 2091−2102.




https://dx.doi.org/10.1021/jacs.1c00557
J. Am. Chem. Soc. 2021, 143, 4379−4386